



Image-Based Wavefront Sensing and Control Experiments

A selection of experiments conducted on the NGST
Wavefront Control Testbed (WCT-1 and -2) by members
of the NGST WFS&C Government Team

Dave Redding, Scott Basinger, Dave Cohen, Joe Green,
Cathy Ohara, Fang Shi

Jet Propulsion Laboratory

Bruce Dean, Laura Burns

Goddard Space Flight Center

Modes and Algorithms

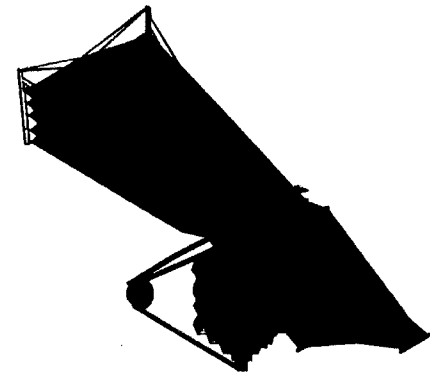
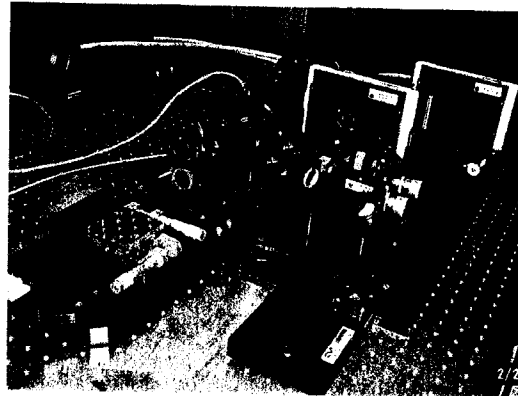
Government Baseline WFS&C System		NGST Performance		Demonstrated in the Lab		TRL
Control Mode	Algorithm	Capture Range (WFE)	Accuracy (rms WFE or WFSE)	Capture Range (WFE)	Accuracy (rms WFE or WFSE)	
Coarse Alignment	Segment ID	5 mm		5 mm		4
	Capture					4
	Coarse Align		10 um		10 um	4
Segment Figure Correction	WFS/Prescription Retrieval	25 um / segment	<10 nm / segment			7
	WFS/High Dynamic Range MGS	25 um / segment	<10 nm / segment			7
	WFC		<100 nm / segment			4
Coarse Phasing	Dispersed-Fringe Sensing	Segment depth of focus	1 um piston error	50 um	100 nm piston error	4
	White-Light Interferometry	10 um	10 nm piston error	5 um	20 nm piston error	4
SM Align	WFS/Prescription Retrieval					3
Fine Phasing	WFS/MGS	5 um	<10 nm	3 um	4 nm WFSE	7
	WFC	5 um	<100 nm	3 um	20 nm	4
Actuator Calibration	WFS/MGS		<10 nm		2 nm	4
Camera-specific WFE Calibration	WFS/MGS		<10 nm		4 nm WFSE	2
PSF Monitoring	IPO/Prescription Retrieval		<10 nm		6 nm	4

NGST baseline WF control approach has several modes of operation (see also paper [4850-49]). Telescope initialization, performed at first light, cascades from *Capture* through *Fine Phasing*, reducing errors from millimeters to nanometers. *Calibration* of the science instruments establishes the separate instrument WF errors and defines the global WFC set points. *PSF Monitoring* will monitor the evolution of the WF error during science operations, to determine when Fine Phasing may need to be repeated.

Experiments shown here illustrate performance of several of these modes.

Hardware

The WCT-1 and -2 testbeds provide small-scale hardware analogs of NGST for WFS&C development, see [4850-55]. The NGST Phase Retrieval Camera provides portable WFS capability for testing large optics, see [4850-61]. A new testbed for the Terrestrial Planet Finder mission with extreme WFC accuracy capabilities is coming on line, see [4854-41]. Experience with these testbeds validates our computer modeling methods, which are applied to simulate the NGST space observatory configurations.

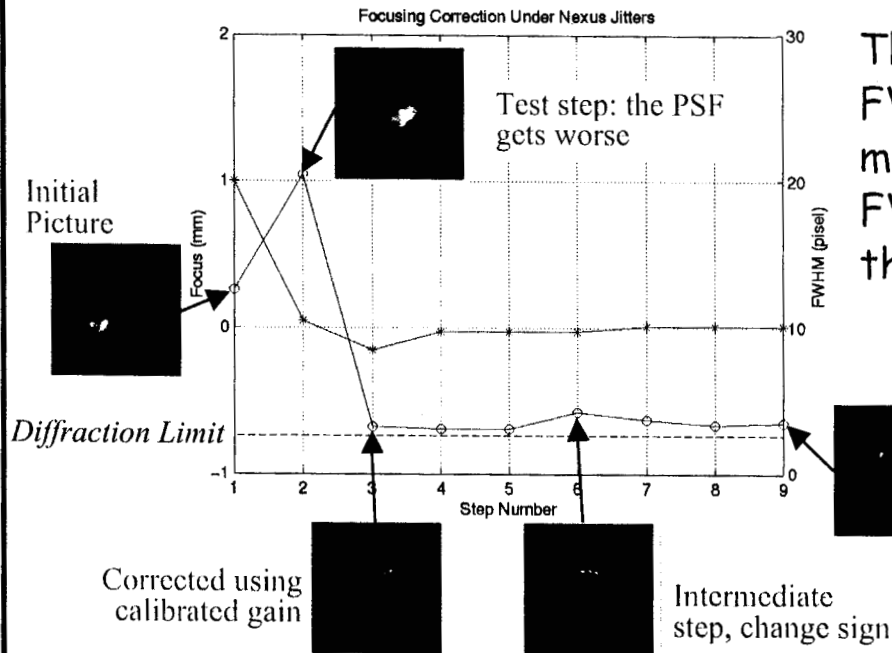


Coarse Alignment/Segment Focusing in Presence of Large Guiding Errors

Fang Shi

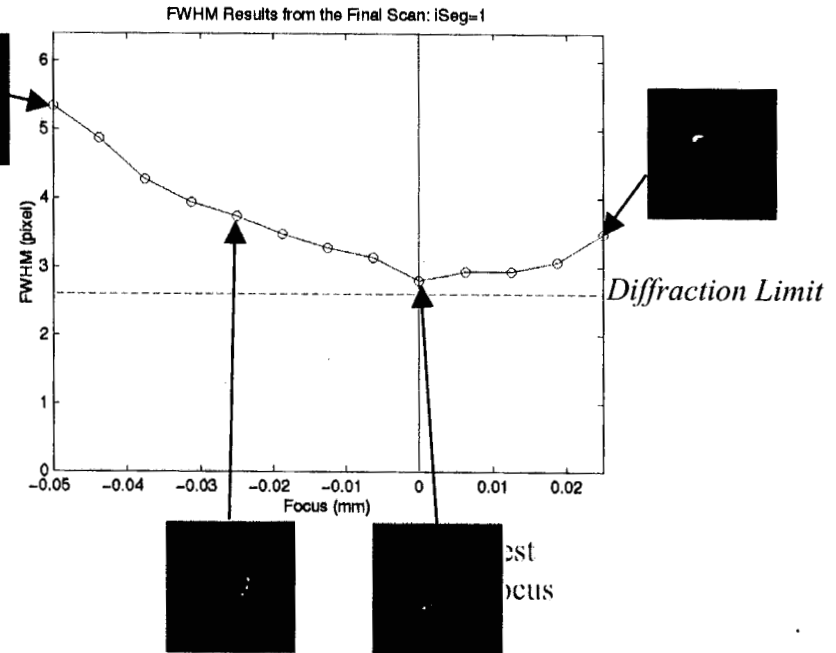
Initial telescope *Coarse Alignment* control uses a Segment Focusing algorithm, which scans the segments to find best focus. Nominally, this step will be performed with the Fine Guidance System running, keeping the telescope pointed to a small fraction of an arcsecond. This experiment examines performance in the unlikely event that Fine Guidance is not active during Segment Focusing. It uses simulated "Nexus" star images; Nexus was a small, 3-segment version of NGST studied as a potential precursor mission.

The focusing algorithm optimizes a "minimum FWHM" metric, rather than the usual "encircled energy," when drift is large. This metric provides accurate guidance even when the PSFs are smeared out into snaky tracks.



This plot shows segment focus error and FWHM during Segment Focusing using the modified FWHM metric. Note that the FWHM is correctly estimated, even though drift smears the PSF

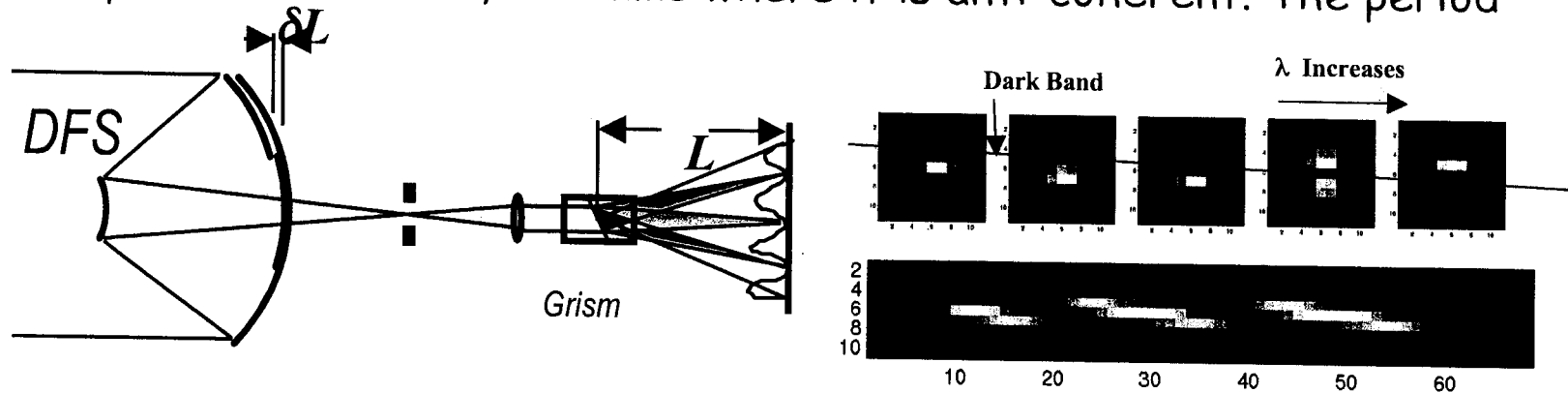
This plot shows FWHM as a function of focus error near segment best focus during a final focus scan, as computed on drifting, snaky PSFs.



Dispersed-Fringe Sensing at Low Light Levels

Fang Shi

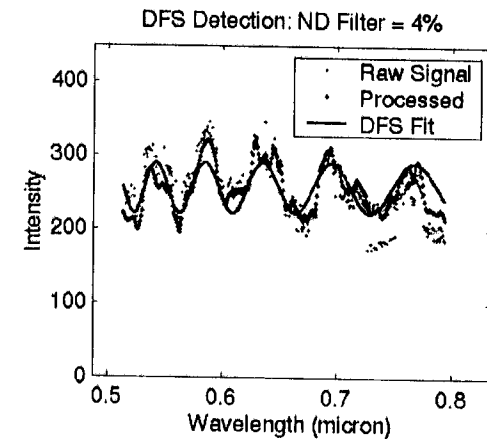
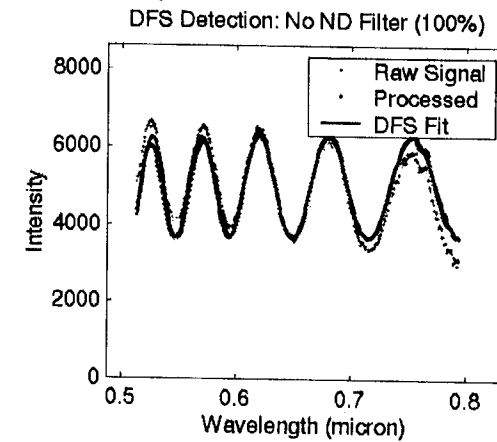
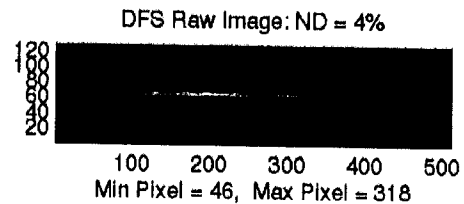
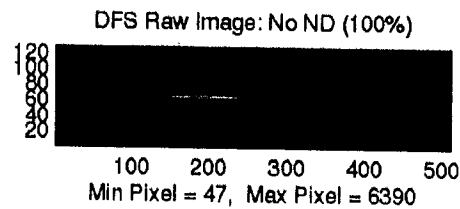
Initial telescope *Coarse Phasing* control uses a *Dispersed-Fringe Sensor* (DFS) algorithm operating on spectra from the NIRcam to measure segment piston errors. The spectra are obtained using a grism slotted in a filter wheel. The spectrum of an un-phased segment is an interference fringe, with peaks where the wavelength is coherent with the piston difference, and nulls where it is anti-coherent. The period



of the fringe gives the absolute value of the piston δL , and the slope of the dark band indicates the sign of δL .

This experiment uses WCT-2 to explore the accuracy of DFS at low light levels. Exposure was adjusted using neutral density filters and short exposure times.

The lowest light level for which DFS produced a reliable measure of piston was at about 4% of nominal. Converting DN to photon flux indicates that SNR~17.



Simulations were carried out using the Nexus NGST precursor mission configuration, with meter-class segments, for comparison with the WCT-2 experiments.

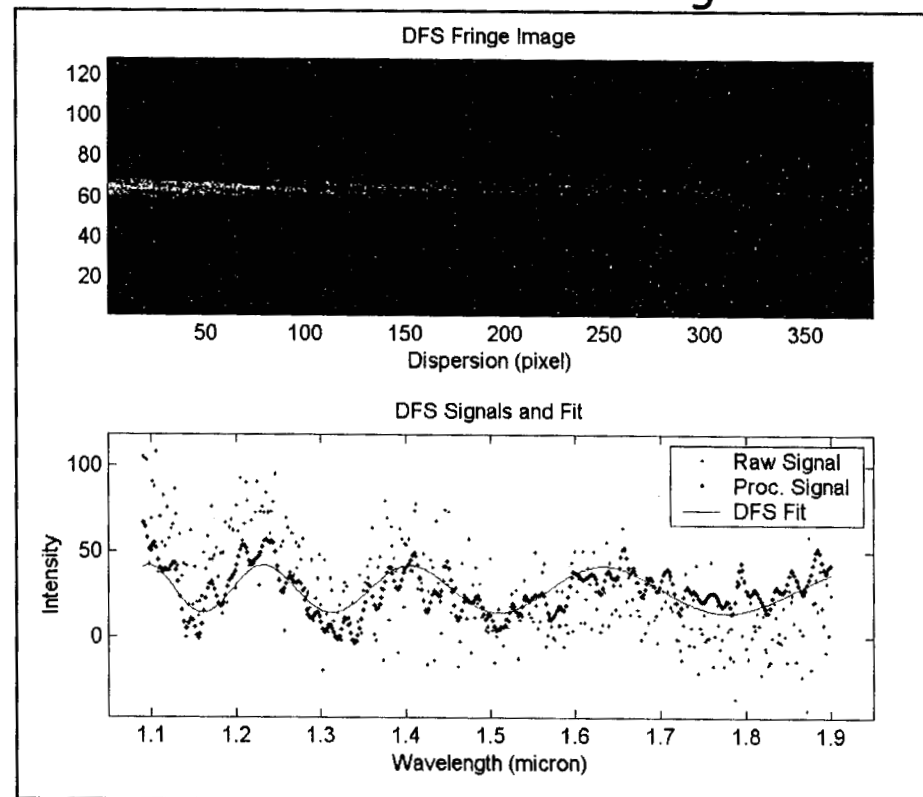
The limiting magnitude for Nexus DFS to reliably detect a 200 nm piston error with exposure times of 1 sec were:

- K7V star: $M_K < 13$ mag
- A0V star: $M_K < 14$ mag

Longer exposures increase the limiting magnitude, but jitter, drift, sky background, detector dark current may limit exposure time.

This work was performed to explore the limits of DFS performance. During NGST alignment and phasing, we should be able to select our observations to maximize performance, and can avoid low light imaging. See [4850-51] and [4850-59] for further details on *Coarse Phasing*.

NEXUS DFS Modeling:



PSF Monitoring vs. Dispersed-Fringe Sensing

Cathy Ohara and Fang Shi

PSF Monitoring is performed during normal science observations, with the actuators turned off. We use an "In-focus PSF Optimizer" (IPO) algorithm to measure the low spatial-frequency wavefront error, using in-focus star images as input, see [4850-64]. This WCT-2 experiment compares IPO to DFS measurements of piston error.

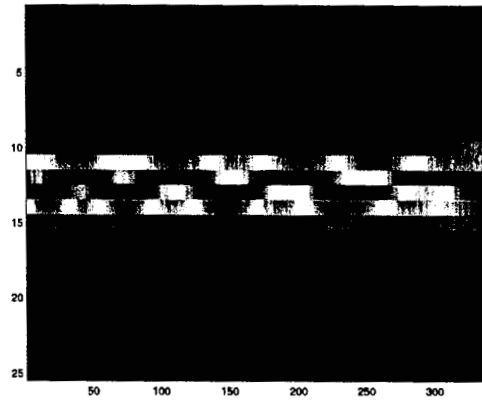
The experiment began by deliberately pistoning one of the WCT-2 segments. DFS fringes were measured, and then the grism was removed from the beam and an in-focus image was taken for IPO.

Before DFS correction:

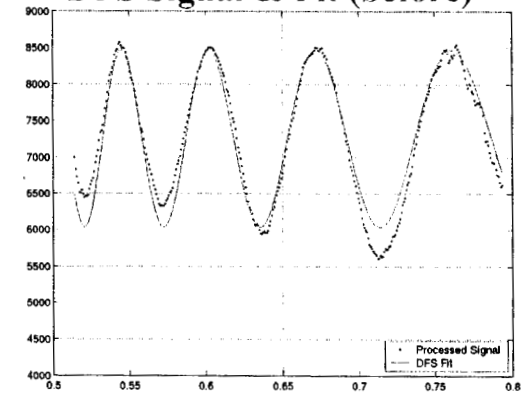
DFS Measured = $-2.959 \mu\text{m}$

IPO + PZT piston = $-3.030 \mu\text{m}$

Before DFS Correction:



DFS Signal & Fit (before)

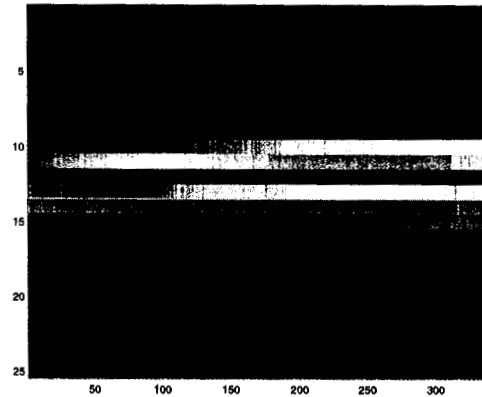


After DFS correction:

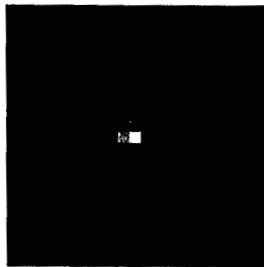
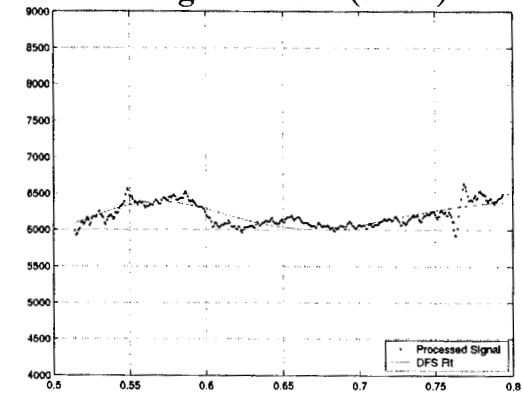
DFS Measured $\sim 0 \mu\text{m}$

IPO Measured = $-0.022 \mu\text{m}$

After DFS Correction:

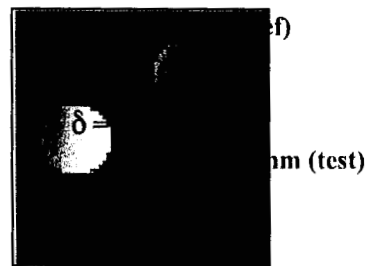


DFS Signal & Fit (after)



IPO Image after DFS correction

IPO WF after DFS correction



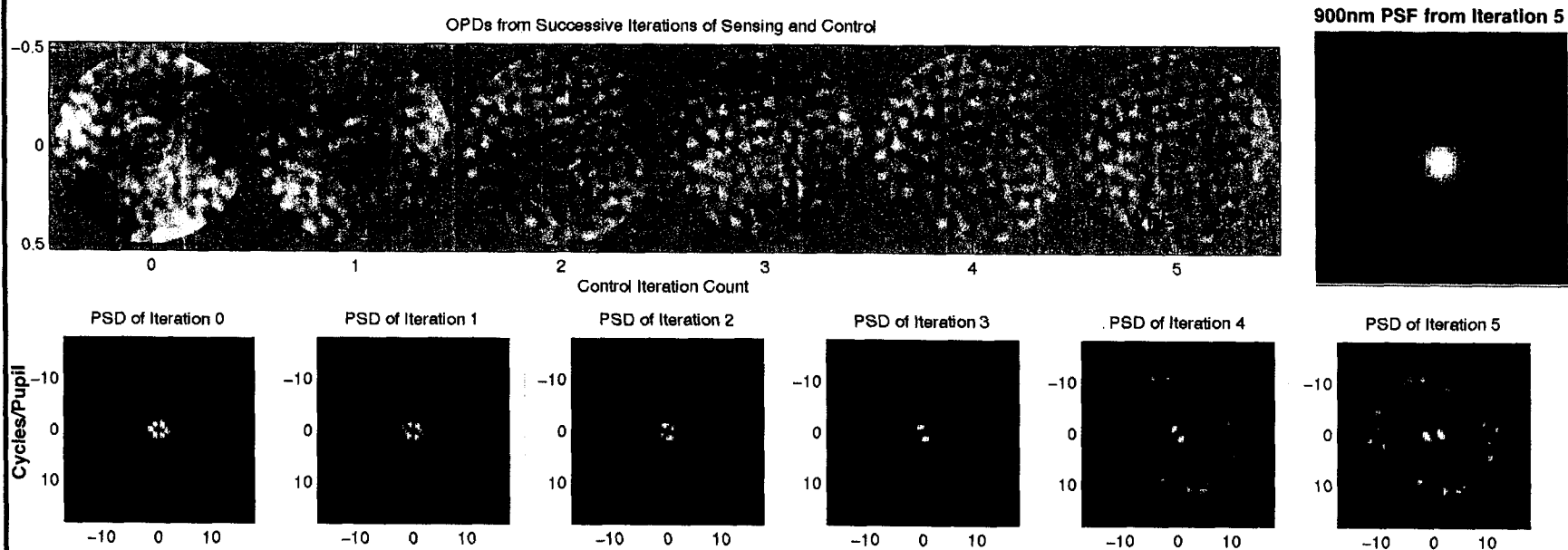
With a proven accuracy of $\sim 6 \text{ nm}$, IPO provides an independent method for verifying DFS accuracy

Wavefront Control via MGS Phase Retrieval

Joseph J. Green

In *Fine Phasing* mode, a Modified Gerchberg-Saxton (MGS) phase retrieval algorithm processes defocussed NIRcam images to measure a wavefront error map. The WF map is then used to move and deform telescope optics to optimize imaging performance.

This experiment explores Fine Phasing accuracy using the WCT-1 testbed in a sequence of 5 WFS&C iterations. Initial WF error, imparted by the "Telescope Simulator Deformable Mirror" (SDM), is small. Corrections are applied using a second, "Adaptive Optics DM" (AODM).



Power Spectral Density (PSD) plots of the successive estimates show that the AODM is effective in removing mid spatial-frequency WF errors. It clears out a "black hole" surrounding the core of the PSF - but leaves a "halo" of scattered light at spatial frequencies beyond $1/(\text{twice the actuator spacing})$, the Nyquist f for the AODM.

More surprisingly, it leaves a finite (though small) amount of low spatial-frequency aberration, which is well within the AODM bandpass. These low- f errors reflect the noise limits of the WCT, set by:

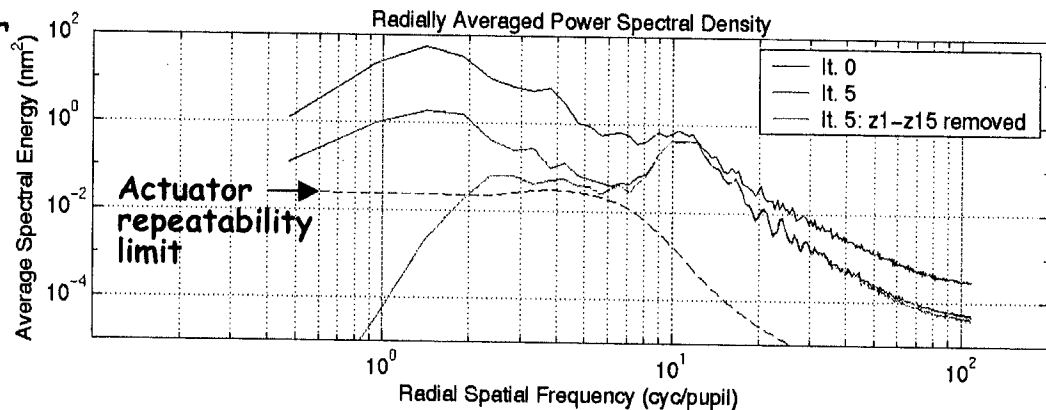
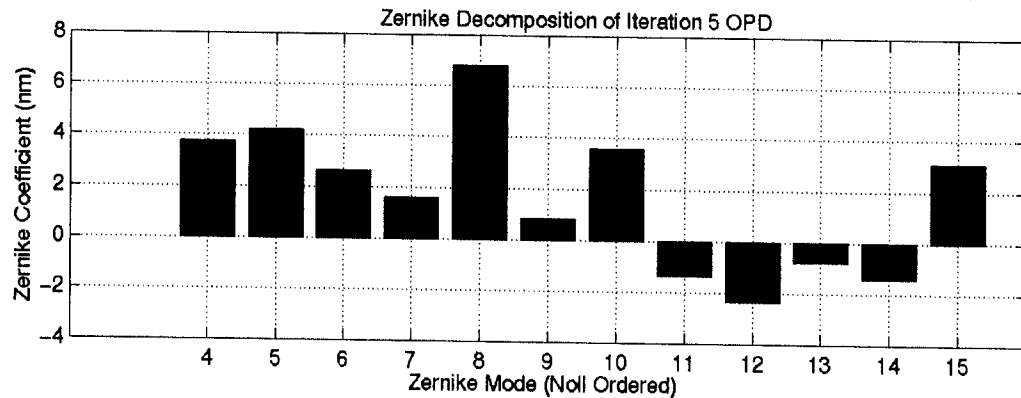
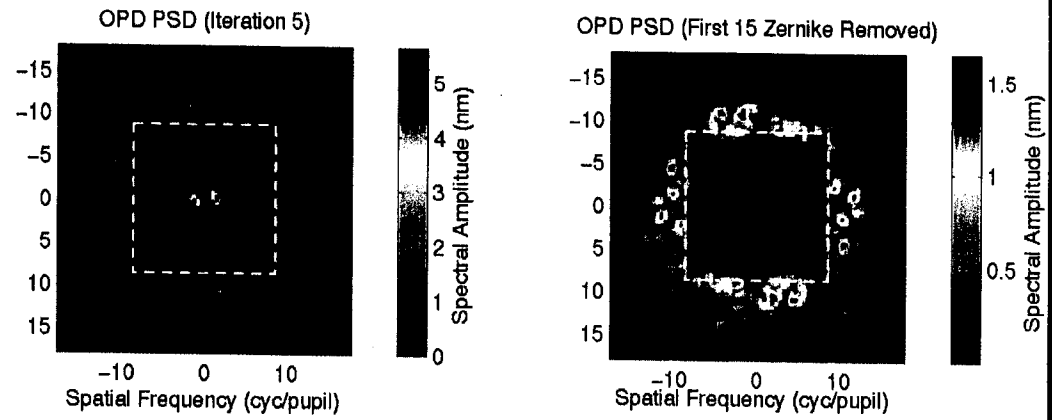
- Lab seeing
- System drifts
- Image centering for MGS
- Vibration
- Defocus stage repeatability
- Aliasing induced by WFC

Removing low-order Zernikes from the estimate, the PSD approaches the ultimate limit imposed by actuator repeatability.

Subsequent improvements to the MGS and WFC algorithms have improved performance. These include:

- Lower WFC control gain
- Anti-aliasing WFC filter
- Sub-pixel image centering for MGS

Other experiments carried out with the NGST Phase Retrieval



Camera (PRC) and a Zygo interferometer in air have established the WF sensing accuracy of the MGS algorithm at better than 3.8 nm [4850-53], and its repeatability at better than 2.5 nm.

A new TPF Testbed coming on line soon will permit testing in a thermally stabilized, vacuum environment, eliminating these major error sources and further helping define the ultimate limits of the NGST Fine Phasing techniques [4854-41].

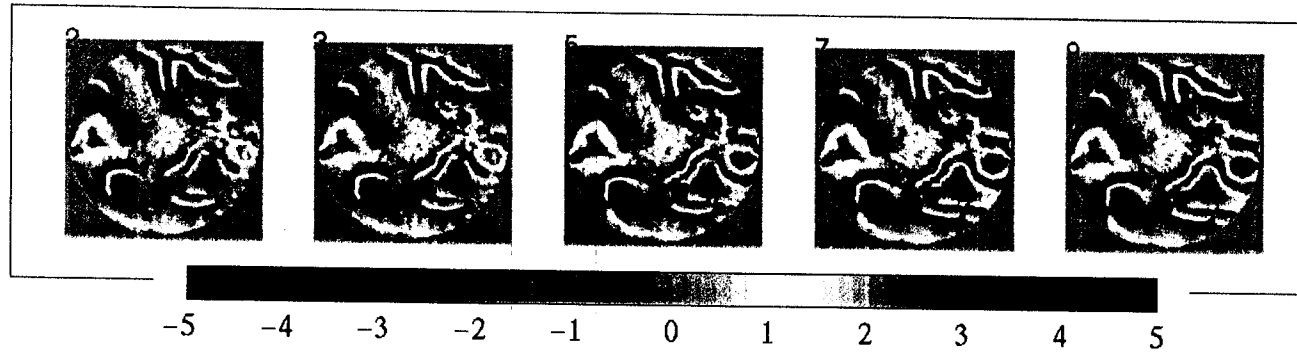
High Dynamic-Range MGS Wavefront Sensing

Dave Cohen

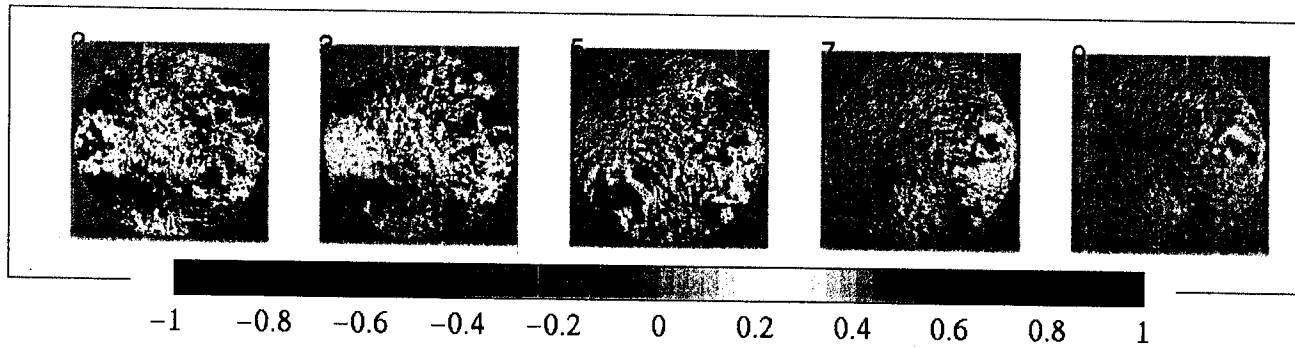
Phase retrieval algorithms such as the MGS measure *wrapped* phase, or phase modulo 2π . For WFC it is necessary to use *unwrapped* WF measurements to compute actuator commands. We have implemented explicit unwrapping as part of MGS, using the algorithm of Ghiglia and Pritt.

This experiment uses the WCT-2 SDM actuators to aberrate the WF in a random pattern of about 3.6λ . The MGS algorithm is iterated 38 times, with unwrapping applied 3 times, following the 9th, 19th and 38th iterations. The evolving estimate, and the guiding error map, are shown:

Prior to first unwrap...

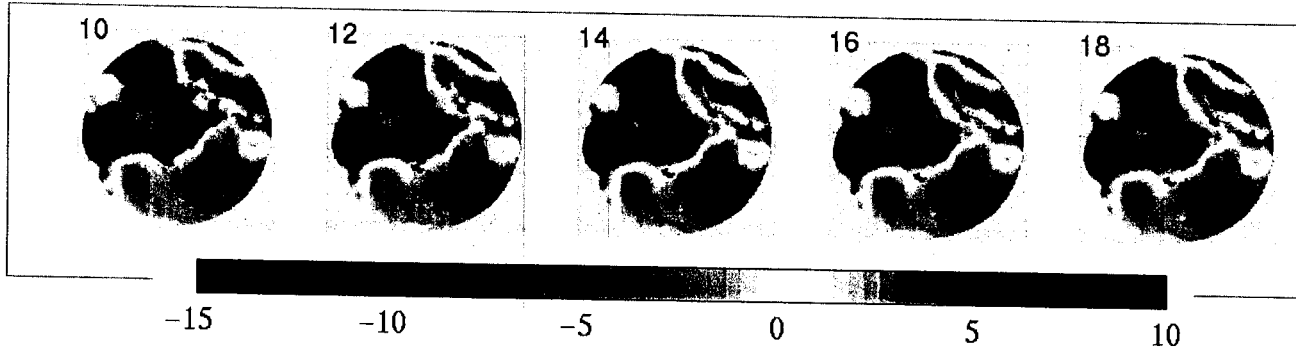


*Exit pupil
phase estimate*

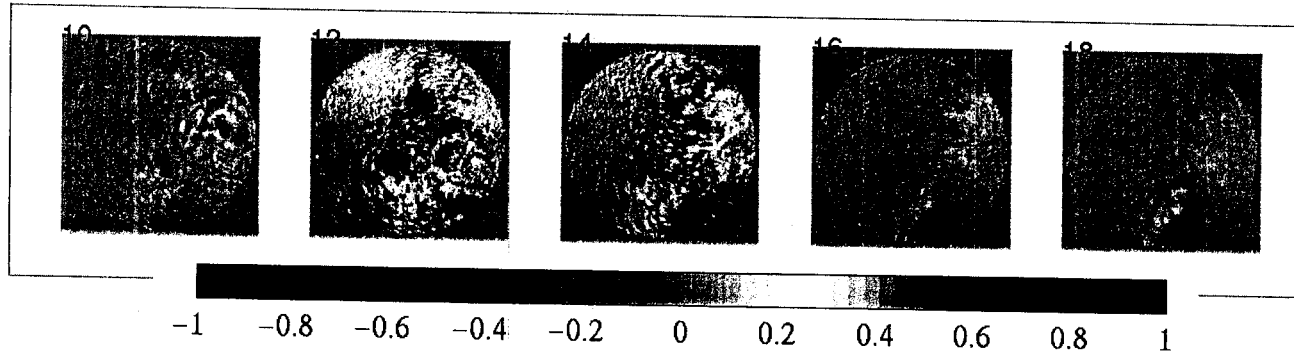


*Calculated
model error*

From first to second unwrap...

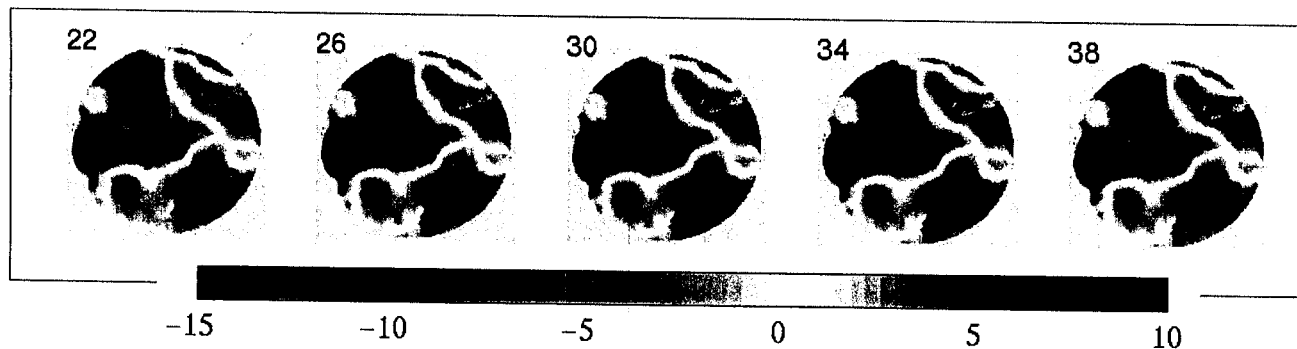


*Exit pupil
phase estimate*

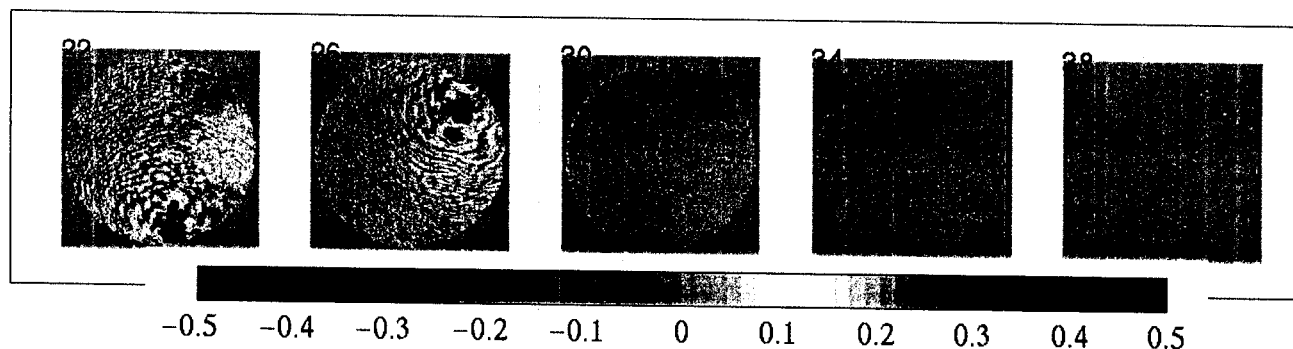


*Calculated
model error*

From second to final unwrap...

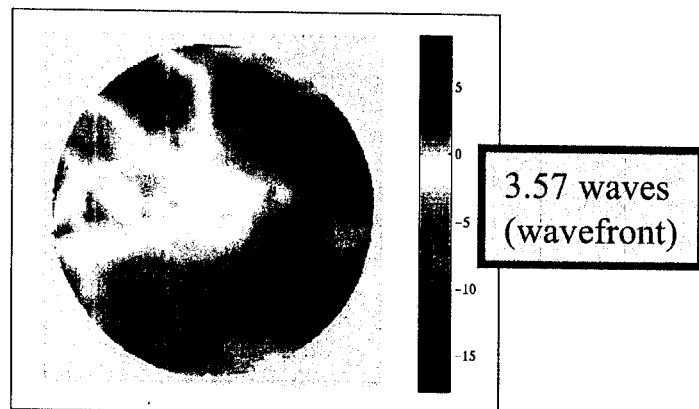


*Exit pupil
phase estimate*

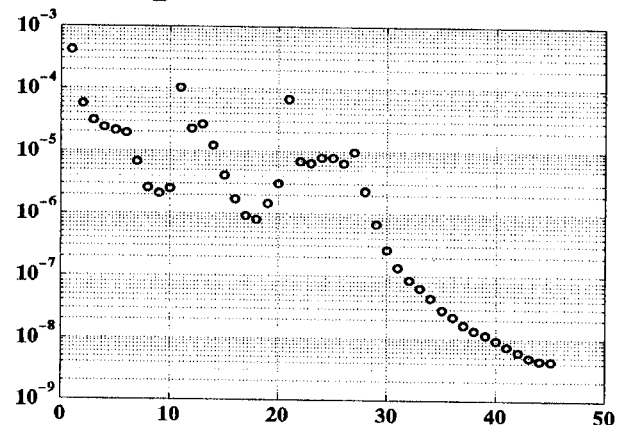


*Calculated
model error*

After final unwrap...



Convergence of X^2 error metric



The capture range of MGS with unwrapping is a few waves. When sensing in the MIRI at a long wavelength (15 μm), this provides a capture range of ~ 50 μm , significantly greater than is required for nominal NGST operations. See [4850-52] for further details.

We use *implicit* unwrapping approaches as well, including *Prescription Retrieval*, which drives a ray-trace model to match defocussed imagery in a classic optimization process. No unwrapping is required in this approach because the solution surfaces are continuous.

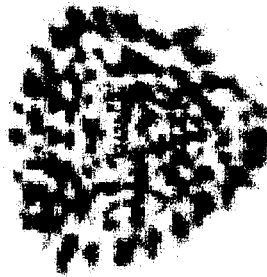
WF Sensing in Broad-band Light

Bruce Dean

Phase retrieval is tolerant of blurring effects, such as the smearing that comes with broad-band light, as illustrated in this experiment. Defocussing moves the mapping of image to pupil into the geometric regime. The intensity variations that signal surface irregularities grow in size with defocus, while the blur "kernel" stays the same size, and so has less overall influence on the estimate.

In this experiment, the WCT-1 AODM was aberrated with about 1 wave of trefoil. Phase retrieval data was taken with 2 filters, one narrow band ($R \sim 100$), the other broad-band ($R \sim 1.75$). The low- f estimates that resulted are very close.

Narrow-band
defocussed
image: $R \sim 105$



Broad-band
defocussed
image: $R \sim 1.75$

